JMEPEG (2009) 18:638–648
DOI: 10.1007/s11665-009-9421-y

1059-9495/$19.00

Conceptual Design and Simulation of a Compact Shape Memory Actuator for Rotary Motion

I. Spinella, G. Scirè Mammano, and E. Dragoni

(Submitted September 15, 2008; in revised form February 23, 2009)

This work describes the conceptual design, the modelling, the optimization, the detail design and the virtual testing of a shape memory actuator purposely conceived to maximize torque and angular stroke while limiting overall size and electric consumption. The chosen design, achieved by means of a Quality Function Deployment approach, features a fully modular concept in which an arbitrary number of identical modules are assembled to produce the desired angular stroke and output torque. The basic module contains shape memory springs that actuate the device and also a conventional spring that reduces the torque ripple. Following the concept generation stage, a thermo-electromechanical model is developed and a numerical optimization performed, aimed at minimizing the electrical consumption of the actuator. Finally, the device is designed in detail and the actuator is tested virtually. Thanks to the proposed modular construction and the use of a conventional balancing spring, the device shows better performances than known rotary shape memory actuators in terms of rotation, torque and customization.

Keywords conceptual design, modeling, rotary actuator, shape memory alloys, simulation

1. Introduction

Shape memory alloys (SMAs) are increasingly exploited to build actuators and micro-actuators for many applications. The chief advantages of these smart materials are the very high power versus mass and force versus mass ratios and the small amount of active material needed for the actuation. Moreover, SMAs allow to simplify the kinematic chain, to obtain a silent and clean actuation and to work in corrosive environment.

Although the use of SMAs as actuators is rising, these materials are basically confined to the field of linear devices. By contrast, SMA technology is virtually unexplored for the construction of compact rotary actuators able to provide high output torque and significant rotations. Furthermore, both in linear and in rotary SMA actuators, the electrical consumption and the bandwidth of the SMA actuator are seldom considered as constraints of the design, although the correct choice of these parameters is fundamental to obtain a useful device.

With regard to linear SMA actuators, many applications have been developed in the recent years and some works adopt rational approaches to design the devices. In Ref 1, Colli et al. propose the system design of a linear SMA actuator for automotive tumble flap: the rational Quality Function Deployment (QFD) approach is adopted for the design of the actuator, but the electrical power required for the actuation is excessive and the bandwidth is poor. Huang (Ref 2) shows possible selection criteria for SMA actuators, but no criteria are given about the required electrical power and about the bandwidth. In Ref 3, Reynaerts and Van Brussel propose a design methodology that considers even the cooling time of the actuator, but the design is focused just on SMA wires. The modelling and the simulation of some linear SMA actuators is proposed by Lu et al. (Ref 4), but no rational approaches are adopted to design these actuators. A complete and rational design of a linear actuator based on SMA wires is proposed by Khidir et al. (Ref 5). Even cooling time aspects are considered in this efficient actuator, which is a good example of linear SMA device.

With regard to rotary SMA actuators, just a few applications have been developed. Abadie et al. (Ref 6) develop a rotary SMA actuator cooled by Peltier elements. This actuator does not seem to have many practical applications, because its output torque and angular stroke are poor. Moreover, no electrical efficiency aspects are considered. The same limitations affect the device developed by Gabriel et al. (Ref 7). Kuribayashi (Ref 8) propose another small rotary actuator. The design approach is a rational one, but the same problems highlighted in Ref 6, 7 affect this device. A rotary actuator that supplies a considerable amount of output torque is proposed by Grant and Hayward (Ref 9), but this SMA device is not compact enough to compete with conventional actuators successfully.

The analysis of the state of the art shows that there is a lack of work focused on the rational design of compact SMA rotary actuators, able to supply a considerable amount of output torque and to exploit a wide angular stroke, minimizing at the same time the electrical consumption. Aimed at filling this gap, this work deals with the design, the optimization and the dynamic simulation of a rotary SMA actuator specifically studied to minimize the electrical consumption. Simultaneously, the output

This article is an invited paper selected from presentations at Shape Memory and Superelastic Technologies 2008, held September 21-25, 2008, in Stresa, Italy, and has been expanded from the original presentation.

I. Spinella, G. Scirè Mammano, and **E. Dragoni**, Dipartimento di Scienze e Metodi dell'Ingegneria, Università di Modena e Reggio Emilia, Reggio Emilia, Italy. Contact e-mail: igor.spinella@unimore.it.

Nomenclature

α_D	extreme angular position of the cursor	K_{SC}	cold stiffness of active springs
α_P	angular pre-stretch of each active spring	K_{SH}	hot stiffness of active springs
α_{tot}	total angular stroke of the actuator	L_{0S}	free length of the SMA springs
$\gamma_{adm\,s}$	admissible shear strain of the shape memory material	L_{0T}	free length of the conventional spring
$\gamma_{max\,s}$	maximum shear strain of the shape memory material	m	mass of the SMA spring
ν	Poisson ratio of the conventional spring	M_F	martensite finish temperature
ρ	electrical resistivity of the SMA springs	M_S	martensite start temperature
ξ	SMA density	n	total number of elastic units
τ_{adm}	admissible shear stress of the conventional spring	N_S	number of SMA springs active coils
X_{AM}	enthalpy of the transformation from austenite to martensite	N_T	number of conventional spring active coils
		O	centre of the basic module of the actuator
X_{MA}	enthalpy of the transformation from martensite to austenite	P	electric power
		P_{adm}	admissible value of the electric power
A_F	austenite finish temperature	P_M	maintenance electric power
A_S	austenite start temperature	P_P	peak electric power
b	arm of the force of the elastic unit	R	electrical resistance of the SMA spring
B	mobile cursor of the basic module of the actuator	S	surface of the SMA spring
c	generic specific heat of the SMA	s_1	dimensionless parameter to model the SMA properties
c_A	austenitic specific heat of the SMA	S_1	shape memory spring 1 of the elastic group 1
c_{AM}	austenite to martensite specific heat of the SMA	S_2	shape memory spring 2 of the elastic group 1
c_M	martensitic specific heat of the SMA	S_3	shape memory spring 1 of the elastic group 2
c_{MA}	martensite to austenite specific heat of the SMA	S_4	shape memory spring 2 of the elastic group 2
C_S	spring index of the SMA springs	t_{adm}	admissible cooling time of the SMA springs
C_T	spring index of the conventional spring	t_{cool}	cooling time of the SMA springs
d_S	wire diameter of the SMA springs	t_{ON}	activation time
d_T	wire diameter of the conventional spring	t_R	rising time of the SMA springs
D_{adm}	admissible diameter of the rotary actuator	T_a	ambient temperature
D_S	pitch diameter of the SMA spring	T_D	external dissipative torque
D_T	pitch diameter of the conventional spring	T_M	maintenance temperature of the SMA springs
E_C	elastic modulus of the conventional spring	T_P	peak temperature of the SMA springs
E_D	energy dissipated in an actuation cycle	T_{max}	maximum output torque
f_{max}	maximum deflection of the SMA springs	T_{min}	minimum output torque
f_{min}	minimum deflection of the SMA springs	V_{adm}	admissible voltage
G_A	austenite shear modulus	V_M	maintenance voltage
G_M	martensite shear modulus	V_P	peak voltage
h	total convective heat transfer coefficient	$\mathbf{X}$	vector of design variables

torque, the angular stroke and the total size are chosen to obtain an SMA device that can compete with conventional rotary actuators. A QFD approach has been adopted to ensure a quality device, which is able to respect the customer needs for its lifetime. The disclosed rotary SMA actuator shows good performance in terms of output torque, angular stroke, total size and electrical consumption. Moreover, capitalizing on the modular architecture, the angular stroke and the output torque are easily adjusted to meet the requirements of many specific applications.

The development of the actuator is carried out in three steps. In the first step, a structured conceptual design procedure is performed, following the QFD approach. Output of the first step is a concept able to satisfy all the identified customer needs. The second step is focused on the modelling and on the numerical optimization of the concept, which is the output of the first step. Finally, in the third step, the detail design and the virtual testing of the device are accomplished to ensure that the performances of the actuator are able to satisfy the customer needs. The following presentation of the design is organized according to the above division of the work.

2. Conceptual Design

The conceptual design of the actuator was accomplished following the structured QFD approach, as described by Ulrich and Eppinger (Ref 10). Main steps of the conceptual design process are the following:

- definition of the House of Quality;
- functional decomposition;
- generation, evaluation and selection of concepts.

2.1 House of Quality

The House of Quality (HOQ) is a graphical way to arrange the customer needs, the metrics, the competitor performances and the target specifications. Figure 1 shows the complete HOQ of the SMA rotary actuator.

The customer needs (left column of the HOQ) were identified for the commodity field of automatic roll-up shutters. The conventional actuators of this commodity field show

House of Quality	N	1	2	3	4	5	6	7	8	9	10	11	12	13	14	15	16	17	18	Competitors			
	Metrics	Maximum Dimension	Thickness	Torque density	Angular stroke	Price	Bidirectional	SMA technology	Nominal torque	Power consumption	Ripple torque	Adjustable nominal torque	Adjustable angular stroke	Lifetime	Maintenance	Degree of protection	Sound power level	Nominal voltage	Angular Speed	BELIMO CM 24	BELIMO LF24	ARIS N1	SIEMENS 121.1
N Customer Needs	Importance	5	5	5	5	5	5	5	3	3	3	3	3	3	3	1	1	1	1				
2 It is compact	5	•	•	•																+	~	-	+
3 It supplies a high angular stroke	5				•								o							+	-	+	-
4 It is inexpensive	5	o				•														?	?	?	?
5 It is bidirectional	5						•													+	+	+	+
6 It exploits SMA technology	5							•												-	-	-	-
7 It supplies a high output torque	3								•											~	+	+	+
8 It is with low power consumption	3									•										+	~	-	+
9 It supplies a smooth motion	3										•									+	+	+	+
10 It is modular	3											•	•							-	-	-	~
11 It is reliable	3													•	•	•				+	~	~	~
12 It is safe	1															•				+	+	+	+
13 It is silent	1																•			+	-	?	?
14 It exploits electric energy	1																	•		+	+	+	+
15 It is fast	1																		•	-	~	+	-
Measurement Unit		mm	mm	Nm/dm^3	deg	€	Bin	Bin	Nm	W	Nm	Bin	Bin	Cycles	List	IP	dB	V	deg/s				
BELIMO CM 24		158	16	14.1	315	nd	YES	NO	2	0.5	nd	NO	NO	100k	Free	54	35	AC-DC 24	1.2				
BELIMO LF24		155	64	4.1	95	nd	YES	NO	4	5	nd	NO	NO	60k	Free	54	62	AC-DC 24	2.4				
ARIS N1		146	120	2.2	330	nd	YES	NO	5	50	nd	NO	NO	nd	Free	54	nd	AC 230	6				
SIEMENS 121.1		192	60	7.5	90	nd	YES	NO	7	3.5	nd	YES	NO	nd	nd	54	nd	AC-DC 24	1				
Target Value		≤150	≤60	≥ 4	≥60	100	YES	YES	≥2	≤10	≤30%	YES	YES	50k	Free	54	35	DC 24	≥5				

Competitors performances	
Symbol	Performance
+	Good
~	Neutral
-	Bad

Interrelationship among customer needs and metrics	
Symbol	Interrelationship
•	Strong
o	Weak

Fig. 1 House of Quality of the SMA rotary actuator

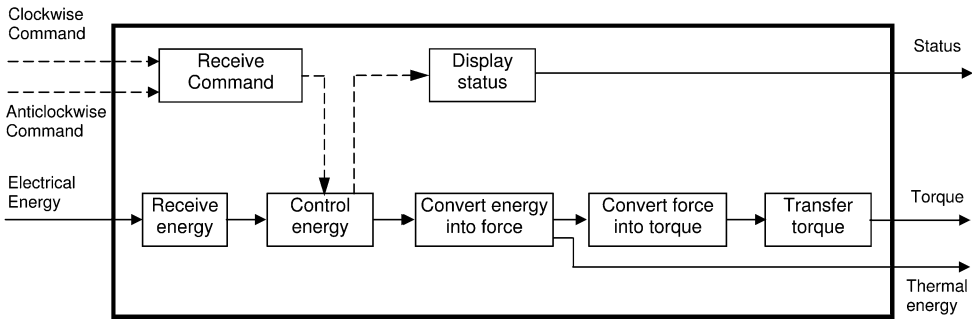

Fig. 2 Functional diagram of the SMA rotary actuator

excellent performances. For this reason, the design of an SMA device able to compete with these products is a good way to show the potential of the SMAs in the field of rotary actuators. Associated with the customer needs, a set of metrics was developed (top row of the HOQ), aimed at defining quantitative characteristics that help to lead the design toward the achievement of the customer needs. Then, the performances of the competitors found in the field of automatic roll-up shutters were studied (relative to both customer needs and metrics) to define the target specifications of the SMA rotary actuator (right column and lower row of the HOQ, respectively).

Relevant target specifications reported in the HOQ are total angular stroke = 60°, nominal output torque = 2 Nm, maximum dimension = 150 mm.

2.2 Functional Decomposition

The functional diagram is a graphical way to show the critical functions of a system and the relationships among these functions. Figure 2 shows the high-level functional diagram of the SMA rotary actuator. The diagram is focused on the critical functions that were identified: ''Convert energy into force'' and ''Convert force into torque''.

2.3 Generation, Evaluation and Selection of Concepts

A concept generation stage process was exploited to find solutions to each critical function. This process was undertaken by means of external research (to take inspiration from former solutions) and by means of internal research (to generate original ideas). Group-oriented techniques as brainstorming and 6-3-5 method were used (Ref 11). Finally, a combination of the concept fragments led to a portfolio of global concepts.

The evaluation and the selection of the global concepts were performed in three steps. Firstly, the global concepts were evaluated by means of a qualitative screening matrix. Then, a critical revision and an improvement of some global concepts

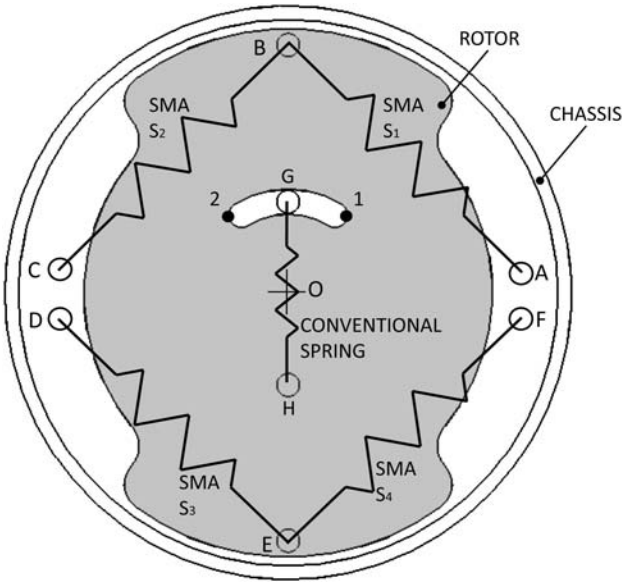

Fig. 3 Final concept for the basic actuator module

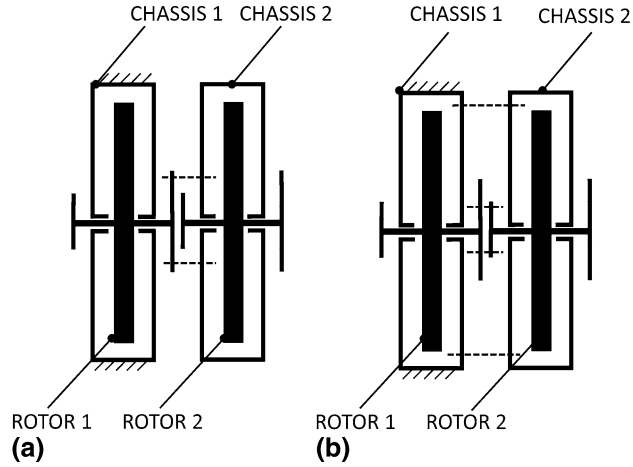

Fig. 4 Angle assembly (a) and Torque assembly (b) of two basic modules

were performed. Finally, a quantitative scoring matrix was used to choose the best concept.

Figures 3 and 4 display the final concept that was chosen for further development. The system is fully modular. The basic modules of Fig. 3 can be assembled to increase the angular stroke, as shown in Fig. 4(a), or to increase the output torque, as shown in Fig. 4(b). Proper combination of the right number of elementary modules, arranged according either to Fig. 4(a) or (b), can thus match any requirement in terms of output torque and angular stroke. The basic module is made of an outer chassis (white ring in Fig. 3), an inner rotor (grey area in Fig. 3) and an arbitrary number, n, of spring units, joining the rotor to the chassis. In Fig. 3 just two units are represented for clarity, one unit formed by SMA springs S_1 and S_2, and the other formed by SMA springs S_3 and S_4. Each SMA spring is linked to the chassis (points A, C, D and F, respectively) and to the rotor (points B and E). Only one spring of each elastic unit is warmed at a time: for example, if S_1 and S_3 are activated, S_2 and S_4 are not activated and vice versa. When S_1 and S_3 are activated, a clockwise motion occurs. On the contrary, when S_2 and S_4 are activated, an anticlockwise motion takes place.

In addition to the SMA spring units, the basic module contains also a conventional spring (GH in Fig. 3). The spring is linked to the chassis at point G and to the rotor at point H. This spring is introduced to reduce the torque ripple of the actuator. In fact, when SMA springs S_1 and S_3 are activated starting from the extreme position 1 of Fig. 3, they are fully extended, and for this reason they supply a high value of output torque, which decrease reaching its minimum in the extreme position 2. The conventional spring acts against S_1 and S_3 when they are fully extended, reducing the peak of the output torque, and helps S_1 and S_3 when they are near the extreme position 2. The same reasoning applies to springs S_2 and S_4.

Warming of the SMA springs is achieved by means of Joule effect, when a suitable current is supplied to them. To this aim, an electronic board on each module receives the commands (see Fig. 2) and applies a voltage to the SMA springs to actuate them properly. An external board controls all the modules of a multistage actuator, deciding the proper commands to provide to each one. This control system allows both the on/off and the proportional control of the actuator. Cooling of the SMA springs is achieved by means of natural convention.

3. Modelling and Numerical Optimization

This section describes the mathematical modelling of the basic module of Fig. 3, which represents the heart of the actuator. As a first step, a thermo-electromechanical model was developed, which was able to predict the behavior of the basic module. Then, the thermo-electromechanical model was optimized numerically to minimize the electrical consumption of the module, subject to the mechanical and dynamic constrains of the HOQ. Finally, based on the optimized configuration, the conventional spring that smoothes out the output torque is calculated.

3.1 Thermo-Electromechanical Model

The model is divided into three parts: mechanical model, thermal model and electrical model.

3.1.1 Mechanical Model. The mechanical model of the basic module is shown in Fig. 5, with only one spring unit displayed for reasons of clarity. Two opposite SMA traction springs S_1 and S_2 act on a cursor B. The cursor B is rigidly linked with the centre O, which is the output shaft of the actuator. For this reason, B can only rotate around O maintaining constant the arm b and its generic polar position is (b, α). The other extremities of S_1 and S_2 are fixed on the chassis of the actuator, points A and C, respectively at a polar position of (a, α_P) and (a, $-\alpha_P$). Thus, the angle $2\alpha_P$ is proportional to the total pre-stretch imparted to the system. The active springs S_1 and S_2 are made of the same shape memory material and are geometrically identical. So, when S_1 and S_2 are at the same temperature and no external moment is applied, B remains on the polar position of Fig. 5(a) (b, 0).

An external dissipative moment T_D, which is always opposite to the velocity of the cursor, acts against the cursor. So, when the cursor moves clockwise, T_D is anticlockwise and vice versa. For a correct design of the system, the module must supply an output moment always higher than T_D.

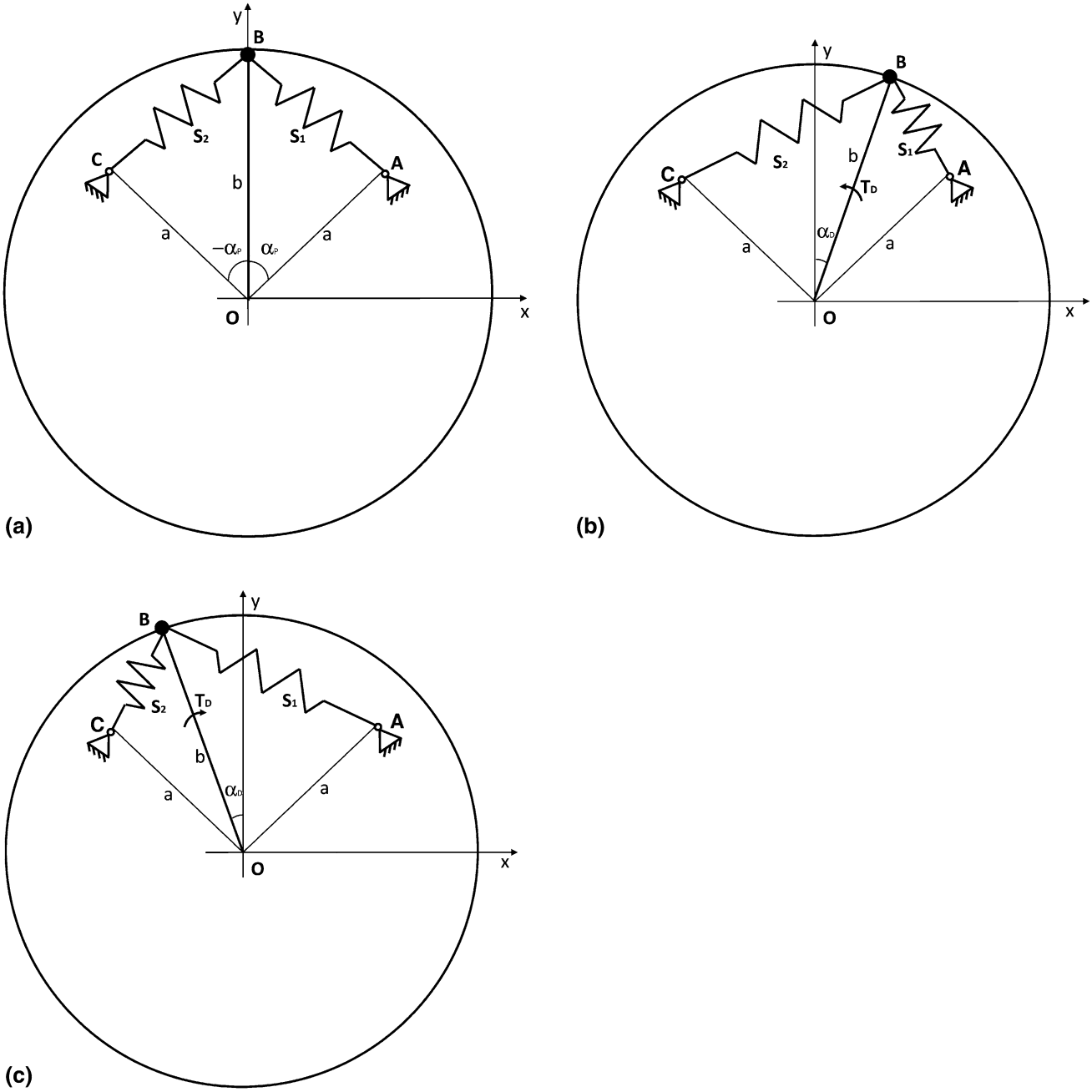

Fig. 5 Mechanical scheme of the basic module: (a) all springs cool, (b) S_1 "hot", (c) S_2 "hot"

When S_1 is warmed up over the austenite finish temperature, A_F, maintaining S_2 below the martensite finish temperature, M_F, the cursor moves clockwise reaching the position (b, α_D), as shown in Fig. 5(b). For the symmetry of the problem, when S_2 is warmed up over A_F and S_1 is cooled below M_F, the cursor moves anticlockwise reaching the position (b, $-\alpha_D$), as shown in Fig. 5(c). As a result, the total angular stroke of the actuator is $\alpha_{tot} = 2\alpha_D$.

Each spring in Fig. 5 is modelled as a helical traction spring exhibiting a linear force-deflection relationship. Although the real stress-strain response of the material can be far from linear in the cold state, assumption of linear behavior is acceptable when only the end positions of the actuator are of interest (Ref 12). Figure 6 shows the characteristic lines of the alloy, identified by austenite shear modulus G_A at high temperature and martensite modulus G_M at low temperature.

An important dimensionless parameter, s_1, can be defined as the ratio between the hot stiffness, K_{SH}, and the cold stiffness, K_{SC}, of each SMA spring. If the geometric changes related to the deformations of the springs do not influence the elastic constant value, s_1 can also be expressed by the ratio between the austenite and martensite elastic moduli of the spring material as follows:

$$s_1 = \frac{K_{SH}}{K_{SC}} = \frac{G_A}{G_M} \qquad \text{(Eq 1)}$$

From Fig. 5(a), by requesting equilibrium of the rotor under the moments about axis O and applying simple geometrical

relationships, the expression of the output moment can be calculated as a function of the angular coordinate α of point B. From this expression, by substituting $\alpha = \alpha_D$ and considering S_1 in a hot state (stiffness $K_{SH} = s_1 K_{SC}$) and S_2 in a cold state (stiffness K_{SC}), the value of the minimum output moment, T_{min}, can be determined as

$$T_{min} = nabK_{SC}\left(\frac{s_1 \sin(\alpha_P - \alpha_D) f_{min}}{(b - a\cos(\alpha_P - \alpha_D))\sqrt{1 + \frac{a^2 \sin^2(\alpha_P - \alpha_D)}{(b - a\cos(\alpha_P - \alpha_D))^2}}} - \frac{\sin(\alpha_D + \alpha_P) f_{max}}{(b - a\cos(\alpha_D + \alpha_P))\sqrt{1 + \frac{a^2 \sin^2(\alpha_D + \alpha_P)}{(b - a\cos(\alpha_D + \alpha_P))^2}}}\right) \quad \text{(Eq 2)}$$

where f_{max} and f_{min} are the maximum deflection and the minimum deflection, respectively. Using geometric considerations and standard machine design formulas for helically coiled traction springs (Ref 13, 14), these quantities can be written as follows:

$$f_{max} = \left(\sqrt{a^2 + b^2 - 2ab\cos(\alpha_D + \alpha_P)} - L_{0S}\right) \quad \text{(Eq 3)}$$

$$f_{min} = \left(\sqrt{a^2 + b^2 - 2ab\cos(\alpha_P - \alpha_D)} - L_{0S}\right) \quad \text{(Eq 4)}$$

$$L_{0S} = N_S d_S + C_S d_S \quad \text{(Eq 5)}$$

where N_S is the coil number, d_S is the wire diameter, C_S is the spring index of the active springs and L_{0S} is the free length of each spring. All the geometric nonlinearities of the problem were considered in Eq 2-4. Equation 5 takes into account even the size of the spring ends.

Finally, using standard formulas of machine design (Ref 13, 14), the shear strain, $\gamma_{max\ s}$, of the SMA spring can be written as follows:

$$\gamma_{max\,s} = \frac{G_M f_{max}}{\pi d_S N_S C_S^2} \quad \text{(Eq 6)}$$

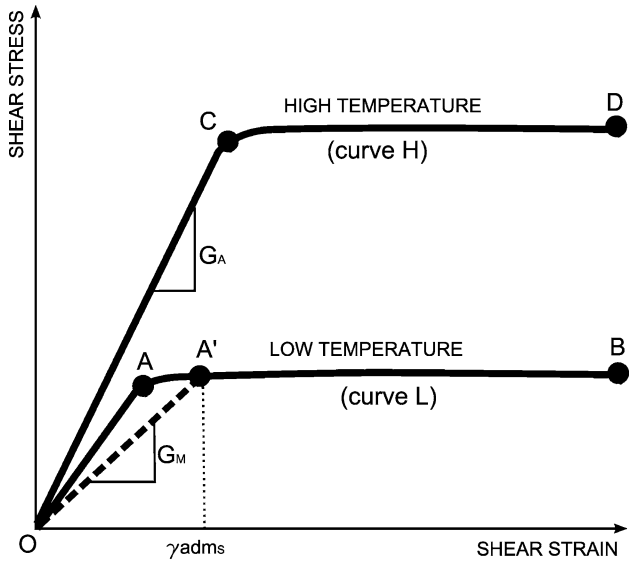

Fig. 6 Simplified shear stress-shear strain behavior of SMAs at different temperatures

3.1.2 Thermal Model. The actuation cycle was assumed like the one shown schematically in Fig. 7. An applied peak voltage, V_P, ensures that the temperature of the SMA spring increases to T_P, just above A_F, in a rising time, t_R. Then, the applied voltage falls to a lower maintenance value, V_M, that ensures a temperature, T_M, slightly above M_S. Due to the hysteresis of the SMAs, the SMA spring remains in austenitic state, thus its shear modulus is still G_A. This approach helps to reduce, at the same time, both the dissipated energy, E_D, and the cooling time t_{cool}. Cooling of the spring is performed by turning off the voltage. With no voltage applied, the temperature decreases from $T_M \approx M_S$ to M_F in the least time that allows the complete transformation from austenite to martensite to be achieved. The value of the activation time, $t_{ON} = 30$ s, was chosen.

The expressions of the rising time, t_R, and the cooling time, t_{cool}, can be obtained using the simplified model proposed by Reynaerts and Van Brussel (Ref 3). The model starts from the consideration that in a polycrystalline SMA

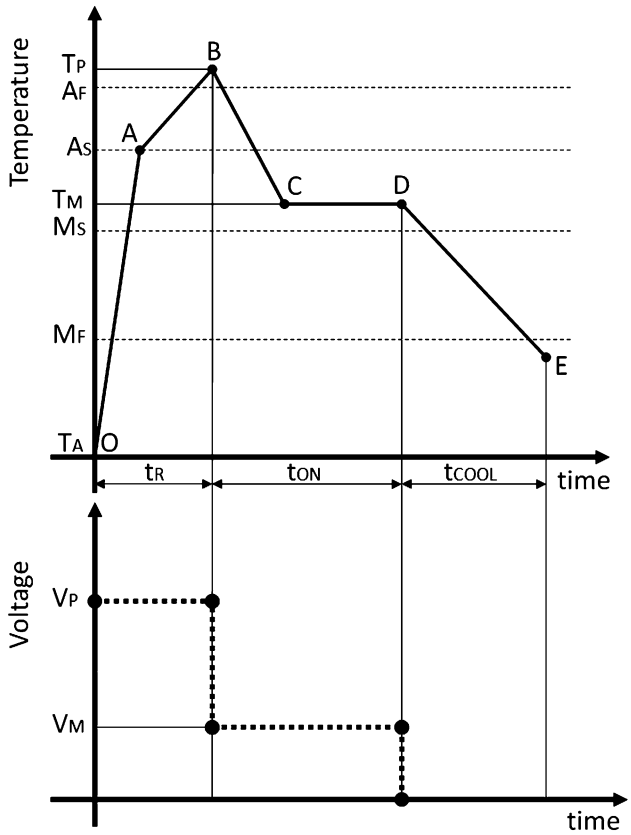

Fig. 7 Actuation cycle

the transformation temperatures, during both heating and cooling, are not precise and well-identified values as it occurs for a single crystal. This is because the transformation temperatures of all the aggregated crystals are not equal but spread over a finite range. When measured for a polycrystal, the martensite to austenite transformation begins at A_S (austenite start) and terminates at A_F (austenite finish). Likewise, the austenite to martensite transformation begins at M_S (martensite start) and terminates at M_F (martensite finish). Throughout both temperature ranges, whenever heat is supplied to or taken away from the polycrystal, the temperature of the SMA varies as it does (though with a different rate) when its state is either entirely austenitic or entirely martensitic. Outside the transformation ranges, the thermal response of the SMA to a net heat input is completely defined by its true specific heats of the material (c_A for austenite and c_M for martensite). Within the transformation ranges, the temperature response is affected not only by the true specific heat (which falls between c_A and c_M) but also by the transformation enthalpies (latent heats) characterizing the polycrystal as a whole during heating (X_{MA}) and during cooling (X_{AM}). Assuming that enthalpies X_{MA} and X_{AM} are absorbed or freed uniformly during the transformations, the thermal effect of those enthalpies can be described by introducing two fictitious specific heats defined as the transformation enthalpies divided by the corresponding transformation temperature interval. By approximating the true specific heat as the mean between c_A and c_M, the global equivalent specific heats throughout austenite to martensite transformation, c_{AM}, and martensite to austenite transformation, c_{MA}, can be written as

$$c_{AM} = \frac{c_A + c_M}{2} + \frac{X_{AM}}{M_S - M_F} \quad \text{(Eq 7)}$$

$$c_{MA} = \frac{c_A + c_M}{2} + \frac{X_{MA}}{A_F - A_S} \quad \text{(Eq 8)}$$

If the assumption of uniform enthalpy absorption or release is not met, relationships (7) and (8) give only average values of the equivalent specific heats. Still, these values provide good predictions of the thermal response of the material whenever (as is the case in this paper) complete transformations are considered.

By virtue of the above approach, the energy balance of the SMA spring at any temperature T is given by the following differential equation (Ref 3)

$$mc\frac{\partial T}{\partial t} + hS(T - T_a) = P \quad \text{(Eq 9)}$$

where c is the (equivalent) specific heat at temperature T, m is the mass, S is the total surface of the SMA spring, h is the total convective heat transfer coefficient and P is the electrical power entering the spring.

With proper choice of c and by applying the appropriate boundary conditions, Eq 9 gives by integration the thermal transient of the SMA spring between any two selected temperatures. From this transient, the heating or the cooling time required to bring the spring from one temperature to the other is easily found.

Consider, for example, the cooling phase of the spring, ranging from initial temperature $T = T_M \approx M_S$ and final temperature $T \approx M_F$ (line DE in Fig. 7). Integrating (9) between M_S and M_F with $c = c_{AM}$ (austenite to martensite transformation) and $P = 0$ (no power supply) gives the cooling time, t_{cool}, as

$$t_{cool} = \frac{mc_{AM}}{hS}\left\{\ln\left(\frac{M_S - T_a}{M_F - T_a}\right)\right\} \quad \text{(Eq 10)}$$

For the heating phase (line OAB in Fig. 7), the procedure is similar but integration of (9) is most conveniently divided into two parts. The first part (line OA) starts at $T = T_a$ and terminates at $T = T_S$ during which the (true) specific heat is $c = c_M$. The second part (line AB) starts at $T = T_S$ and terminates at $T = T_P \approx A_F$ during which the (equivalent) specific heat is $c = c_{MA}$. Integrating (9) over these two temperature ranges with power supply $P = P_P$ throughout gives the rising time, t_R, as

$$t_R = \frac{mc_M}{hS}\ln\left\{\frac{-P_P}{hS(A_S - T_a) - P_P}\right\} + \frac{mc_{MA}}{hS}\ln\left[\frac{hS(A_S - T_a) - P_P}{hS(A_F - T_a) - P_P}\right] \quad \text{(Eq 11)}$$

The peak and the maintenance temperatures, respectively T_P and T_M, can be obtained by considering a steady state ($\partial T/\partial t = 0$) in expression (9).

$$T_P = \frac{P_P}{hS} + T_a \quad \text{(Eq 12)}$$

$$T_M = \frac{P_M}{hS} + T_a \quad \text{(Eq 13)}$$

In all the above equations, the surface S, the mass m and the convective coefficient h are supplied by the following expressions (ξ = mass density of the SMA)

$$S = \pi^2 C_S N_S d_S^2 \quad \text{(Eq 14)}$$

$$m = \xi\frac{\pi^2 C_S N_S d_S^3}{4} \quad \text{(Eq 15)}$$

$$h = (61.3 - 17.5d_S - 2.7C_S - 0.33N_S + 0.93d_S C_S + 0.08d_S N_S) \quad \mathrm{W\,m^{-2}} \quad \text{(Eq 16)}$$

Expression (16) for the total convective heat transfer coefficient, h, was derived using the numerical procedure reported in Appendix 1.

3.1.3 Electrical Model. It was assumed that each SMA spring is warmed by means of Joule effect. For this reason the simple relationships of a resistor warmed by an applied electrical tension were used, combined with the expressions of the geometry of the SMA springs.

The expressions of the peak electric power, P_P, and the maintenance electric power, P_M, can be written as follows.

$$P_P = \frac{V_P^2}{R} \quad \text{(Eq 17)}$$

$$P_M = \frac{V_M^2}{R} \quad \text{(Eq 18)}$$

In Eq 17 and 18, the resistance, R, of the SMA, can be expressed as

$$R = 4\rho\frac{C_S N_S}{d_S} \quad \text{(Eq 19)}$$

where ρ is the SMA resistivity, calculated as the average between the austenitic and the martensitic state. Equation 19

is a simplified representation of the resistance, which is actually not a constant but a mixture of martensite and austenite contributions that change continuously during heating and cooling. Although this variation is very critical for control applications (Ref 15), it can be regarded as negligible for the optimization and the simulation purposes of this paper.

Finally, in terms of electric powers, P_P and P_M, and actuation times, t_R and t_{ON} (= 30 s), the total energy dissipated in an actuation cycle, E_D, can be expressed as

$$E_D = P_P t_R + P_M T_{ON} \quad \text{(Eq 20)}$$

By combining relationship (20) with Eq 17-19 and 9-16, the total dissipated energy can be cast as a function of the vector of design variables $\mathbf{X} = \{n, N_S, d_S, C_S, a, b, \alpha_P, V_P, V_M\}$.

3.2 Numerical Optimization

A nonlinear numerical optimization was performed to find an optimal configuration of the basic module of Fig. 3 that minimizes the total energy dissipated in the thermal cycle of Fig. 7. Formally, the optimization problem was stated by requesting that vector, $\mathbf{X}$, of design variables

$$\mathbf{X} = \{n, N_S, d_S, C_S, a, b, \alpha_P, V_P, V_M\} \quad \text{(Eq 21)}$$

must be found so as

$$E_D(\mathbf{X}) = \min \quad \text{(Eq 22)}$$

subject to the following mechanical, thermal and electric constrains:

Mechanical Constraints

$$T_{min} \geq T_D \quad \text{(Eq 23)}$$

$$n \leq \frac{\pi}{1.1\alpha_p} \quad \text{(Eq 24)}$$

$$a \leq \frac{0.5 D_{adm}}{1.2} \quad \text{(Eq 25)}$$

$$b \leq \frac{0.5 D_{adm}}{1.2} \quad \text{(Eq 26)}$$

$$\gamma_{max\,s} \leq \gamma_{adm\,s} \quad \text{(Eq 27)}$$

Thermal Constraints

$$T_P \geq A_F \quad \text{(Eq 28)}$$

$$T_M \geq M_S \quad \text{(Eq 29)}$$

$$t_{cool} \leq t_{adm} \quad \text{(Eq 30)}$$

Electric Constraints

$$V_P \leq V_{adm} \quad \text{(Eq 31)}$$

$$V_{ON} \leq V_{adm} \quad \text{(Eq 32)}$$

$$P_P \leq P_{adm} \quad \text{(Eq 33)}$$

in which $D_{adm} = 150$ mm, $\gamma_{adm\,s} = 0.038$ rad, $T_D = 1$ Nm, $t_{adm} = 120$ s, $V_{adm} = 24$ V, $P_{adm} = 250$ W, $A_F = 90$ °C, $A_S = 80$ °C, $M_S = 70$ °C, $M_F = 50$ °C. The values of the transformation temperatures and the shear strain were chosen referring to NiTiNOL.

Constraints (23) to (33) have the following physical meaning. Constraint (23) requires that the minimum value of the output torque must overcome the external dissipative torque. Constraint (24) requires that the angular space taken up by the total number of spring units must be contained in the round angle. Constraints (25) and (26) require that the attachment points of the active springs must fall within the admissible outer diameter of the chassis. Constraint (27) requires that the material of the SMA springs must not be overstretched in torsion. Constraint (28) requires that the austenitic transformation must be completed at the end of the heating up ramp while constraint (29) requires that the martensitic transformation must be prevented throughout the maintenance time (see Fig. 7). Constraint (30) requires that the cooling time must not exceed an accepted value. No constraints were imposed on the rising time, t_R, because it is not critical in comparison with the cooling time. Constraints (31) and (32) require that, by heating up and during temperature maintenance, the applied voltage must not exceed an upper limit imposed by security and practical reasons. Finally, constraint (33) requires that the maximum electric power must not exceed an admissible threshold.

Solving this optimization problem, the minimum value of the objective function $E_D^* = 711$ J was achieved for the following optimal embodiment of the basic module.

$$\mathbf{X}^* = \begin{Bmatrix} n = 2 \\ N_S = 13.43 \\ d_S = 1.42 \text{ mm} \\ C_S = 7 \\ a = 54 \text{ mm} \\ b = 54 \text{ mm} \\ \alpha_P = 1.57 \text{ rad} \\ V_P = 5.2 \text{ V} \\ V_{ON} = 0.7 \text{ V} \end{Bmatrix} \quad \text{(Eq 34)}$$

3.3 Conventional Spring Design

The basic module of Fig. 3 supplies an output torque that is strongly dependent on the angular position. For instance, when the angular position is $-\alpha_D$ (Fig. 5) and spring S_1 is hot, there is a maximum, T_{max}, in the output torque. The torque decreases gradually upon rotation of the actuator and reaches a minimum value, T_{min}, when the angular position is α_D, where spring S_1 achieves its lowest extension. This behavior is shown in Fig. 8.

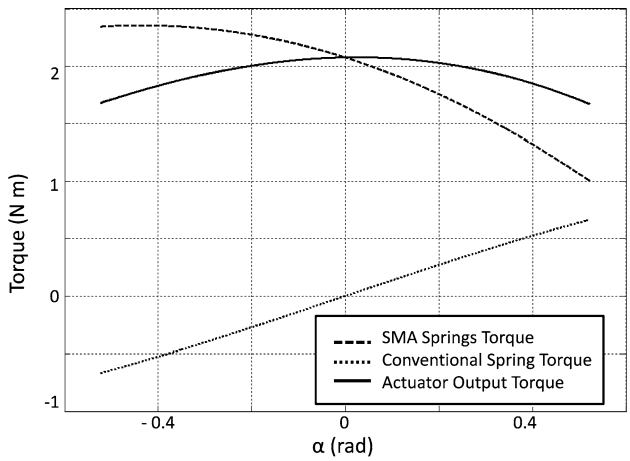

Fig. 8 Diagram of output torque as a function of rotation angle

A conventional spring was thus added to overcome this problem, as shown in Fig. 3 and explained in Sect 2.3. This spring supplies a torque opposite to the one supplied by the hot spring when the hot spring extension is high and a torque that helps the hot spring when the hot spring reaches low extensions. For instance, when S_1 is hot, the traditional spring acts against S_1 for $\alpha = [-\alpha_D \div 0]$, reducing the peak of the output torque, and helps S_1 for $\alpha = [0 \div \alpha_D]$, increasing the minimum output torque. Figure 8 shows that the conventional spring was designed so that the output torque in $\alpha = \alpha_D$ was equal to the output torque in $\alpha = -\alpha_D$, starting from the results of the numerical optimization. To obtain this effect, the spring was designed to ensure a torque which is a half of the difference between the maximum torque, T_{max}, and the minimum torque, T_{min}.

The final result is a reduction in the maximum output torque and an increase in the nominal torque of the actuator (Fig. 8) with a beneficial equalization of the torque profile over the total stroke.

Standard Machine Design formulas (Ref 13, 14) were considered for the embodiment of the spring. The spring is made of steel, with an elastic modulus $E_C = 210000$ MPa, a Poisson ratio $\nu = 0.3$ and an admissible shear stress $\tau_{adm} = 400$ MPa. A numerical optimization was performed to minimize the pitch diameter of the conventional spring. Referring to Fig. 3, the distance between point *G*, fixed to the chassis, and point *H*, fixed to the rotor, was chosen of 40 mm so as not to determine interferences with the other parts of the basic stage. A final spring resulted with wire diameter $d_T = 0.85$ mm, pitch diameter $D_T = 4.3$ mm and $N_T = 9.5$ active coils.

4. Detail Design and Virtual Testing

The detail design of the rotary actuator was performed using a 3D CAD system (SolidWorks) in two steps. In the first step, the basic stage was modelled alone. In the second step, an assortment of multiple-stage actuators was obtained by assembling several basic modules in different ways. Figure 9 presents the result of the first step, with Fig. 9(a) showing a front sectioned view and Fig. 9(b) displaying a rear sectioned view of the module. The circular chassis contains the rotor which is connected to a front disk and to a rear disk. The SMA springs link the chassis to the rotor and provide the actuation of the device. The torque-balancing conventional spring is seen in Fig. 9(a), with one end connected to the chassis (through a circular slot in the rotor) and the other end connected to the rotor. The entire mechanism is protected by a closing lid fitted to the chassis. Several patterns of magnetic sockets are arranged on the rear disk, on the front disk, on the lid and on the rear face of the chassis. Movable steel pins can be inserted into the sockets to provide the double function of connecting adjacent stages in the axial direction and transmitting the torque and the rotation between each other. Insertion of the pins in a particular pattern of sockets determines whether the assembly of two modules will produce the sum of angles (as in Fig. 4a) or the sum of torques (as in Fig. 4b), with the same basic module serving both arrangements. Sliding electric contacts ensure the electric supply of all the stages by allowing the relative rotation of adjacent stages. The supply peak voltage is 5.2 V, the maintenance voltage is 0.7 V and a mean power of 23 W is required.

The final module of Fig. 9 has a diameter of 150 mm and a thickness of 32.5 mm. The reciprocating angular stroke amounts to 60° with a nominal (minimum) output torque of 1.6 Nm and a maximum torque of 2.1 Nm (achieved in the middle position of the angular stroke). The torque density is about 2.8 Nm/dm^3.

The second step of the detail design was devoted to checking the architecture of multistage actuators. To this aim, two basic modules as in Fig. 9 were coupled in angle mode (Fig. 4a) and in torque mode (Fig. 4b) by acting on the proper set of pins (see above). Both configurations were tested to verify the complete functionality of the two-stage actuators in terms of mechanical coupling (correspondence of connecting pins) and electrical connectivity (compliance of siding contacts) through the entire angular stroke.

After the geometric design and the architectural check described earlier, the basic module of Fig. 9 was virtually tested using the kineto-dynamic facility (CosmosMotion) provided by the SolidWorks modeller. The analysis was aimed at verifying that the output torque and the angular stroke of the device

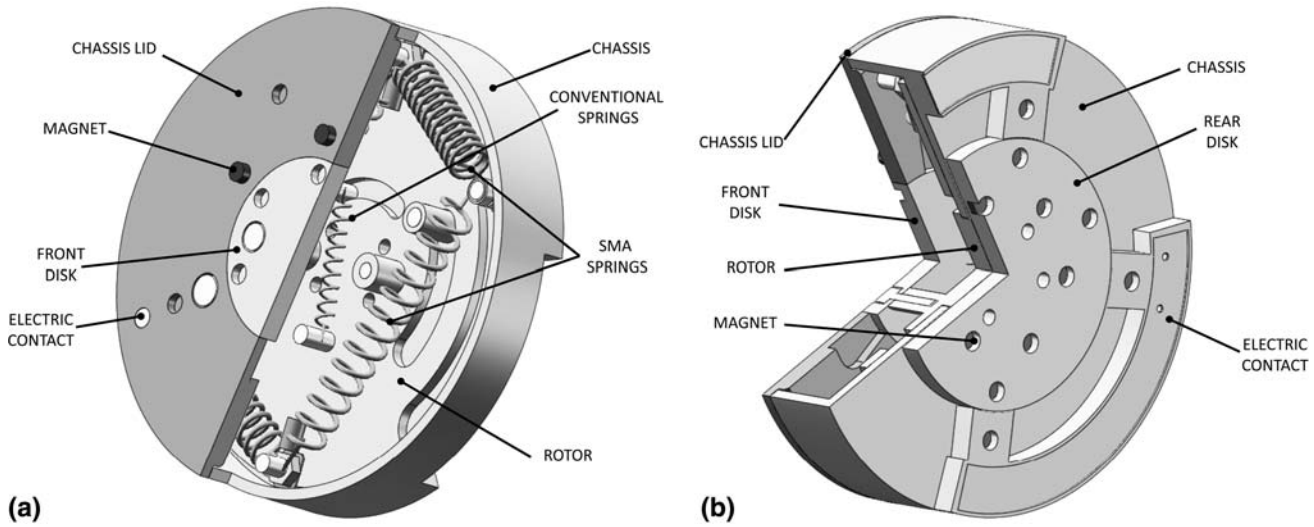

Fig. 9 Detail design of rotary actuator: (a) front view; (b) rear view

would actually meet the target values. The results of the simulations, which are omitted for brevity, fully confirmed the expectations.

5. Discussion

The discussion basically addresses three aspects: the assessment of the actuator performances in comparison with the Target Specifications and with the merits of conventional rotary actuators; the appraisal of the strong and the weak points of the actuator; the suggestion of further work for future developments.

The target specifications related to maximum dimension, thickness and angular stroke of the SMA actuator are fully achieved. Moreover, the nominal torque of the actuator is nearly reached (1.6 Nm instead of 2 Nm). Considering that the actuator thickness is a half of the target specification and that the system is fully modular, the nominal torque target specification can be assumed fully achieved by the assembly of two basic modules coupled together. The designed actuator features a torque density of 2.8 Nm/dm^3 and the target specification was 4 Nm/dm^3. For this reason, this target specification is missed. Likewise also the power consumption specification is not reached with an actual power consumption of 23 W more than doubling the target specification of 10 W. All the other specifications are reached.

The comparison of the SMA rotary actuator with the conventional competitors shows that the proposed SMA design has fair performances in terms of output torque and dimensions. Its performances are acceptable in terms of angular stroke and electric consumption, although their values are worse if compared with conventional actuators. On one hand, the proposed device offers excellent performances in terms of angular stroke, nominal torque, total size and power consumption, if compared with other rotary SMA actuators (Ref 6-9). Furthermore, the proposed methodology is an example of rational and complete design of SMA actuators. The procedure takes into account all the critical aspects that must be considered to design efficient SMA actuators. On the other hand, further work is needed to improve the performance of the present architecture in comparison with conventional competitors. In particular, a mechanical structure must be found that increases the efficiency of the actuator. Although favorable for the achievement of significant strokes, the use of helically coiled SMA springs has limitations in terms of torque generation and can hardly compete with standard actuators. It must be observed, however, that the proposed modular constructions and the use of a conventional balancing spring are very good concepts to enhance angle and torque output. The main conclusion of the paper is that these two key ideas should be retained in the design of future rotary SMA actuators.

6. Conclusions

A shape memory rotary actuator was designed and virtually tested to maximize torque and angular stroke, while limiting overall size and electric consumption. The design process was performed in three steps: conceptual design, modelling and numerical optimization, and detail design and virtual testing. The conceptual design complies with the QFD approach and its output is a global concept that is fully modular: proper combination of the right number of elementary modules can match any requirement in terms of output torque and angular stroke. The basic module is made of shape memory spring units, joining a rotor to a chassis. In addition to these units, the basic module also contains a conventional spring that reduces the torque ripple of the actuator. A thermo-electromechanical model of the basic module was developed and used to perform a numerical optimization, aimed at minimizing the electrical consumption of the actuator. Virtual testing on a 3D digital model confirmed that the output torque and the angular stroke of the device actually meet the target specifications. Although the performances of the present architecture compare unfavorably with conventional competitors, the overall behavior is superior to other shape memory rotary actuators. This improvement is mainly attributable to the proposed modular constructions and to the use of a torque balancing spring: two key ideas that are strongly recommended for the design of future shape memory rotary devices.

Appendix 1

This appendix describes the computational fluid dynamic (CFD) campaign used to determine the total convective heat exchange coefficient, h, of the shape memory spring enclosed in the actuator. For this configuration, the technical literature presents no useful data.

The analyses were performed on the idealized system shown in Fig. 10, with the spring described as a horizontal tube and the enclosing volume described as a horizontal prismatic box with square cross section. The tube represents the envelope of the spring with completely closed coils (mean diameter $D_S = C_S d_S$, wall thickness d_S, axial length $L_S = N_S d_S$). This idealization simplify the CFD problem and ensures conservative results of the heat transfer coefficient with respect to a (stretched) spring with free coils.

The temperature of the tube was set at 373 K (100 °C) and the temperature of the walls of the box was fixed at 293 K (20 °C). The volume of the box was assumed filled with still air at an initial uniform temperature of 293 K (20 °C). In each analysis, the total heat transfer calculated by the software Cosmos Flow Works was divided by the total surface of the

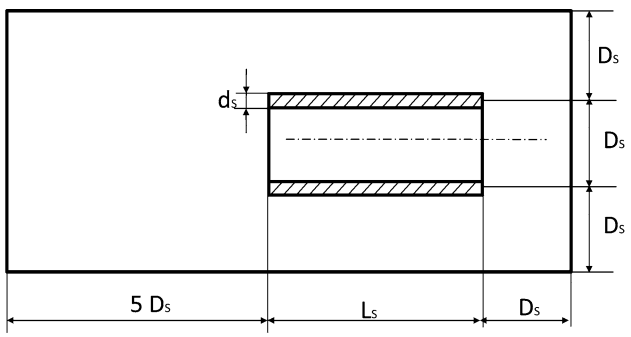

Fig. 10 Geometry investigated in the CFD campaign

tube to obtain the heat transfer coefficient, h, for that particular geometry.

The design of experiments (DOE) approach was adopted to explore the space of all possible spring configurations. Input variables of the DOE were the design parameters of the spring (wire diameter, d_S, spring index, C_S, and coil number, N_S). Two levels were chosen for each variable, and in particular $d_S = 0.25$ and 3 mm, $C_S = 5$ and 12, and $N_S = 12$ and 40.

The values of h calculated for all the configurations were interpolated using statistical instruments to give the polynomial approximation of Eq 15.

References

1. M. Colli, E. Dragoni, and N. Bellato, *System Design of a Shape Memory Alloy Actuator for Automotive Tumble Flap*, SAE Powertrain & Fluid Systems Conference and Exhibition, 2006
2. W. Huang, On the Selection of Shape Memory Alloys for Actuators, *Mater. Des.*, 2002, **23**, p 11–19
3. D. Reynaerts and H. Van Brussel, Design Aspects of Shape Memory Actuators, *Mechatronics*, 1998, **8**, p 635–656
4. A. Lu, D. Grant, and V. Hayward, *Design and Comparison of High Strain Shape Memory Alloys Actuators*, Proceedings 1997 IEEE International Conference on Robotics and Automation
5. E.A. Khidir, N.A. Mohamed, M.J.M. Nor, and M.M. Mustafa, A New Concept of a Linear Smart Actuator, *Sens. Actuators A*, 2007, **135**, p 244–249
6. J. Abadie, N. Chaillette, and C. Lexcellent, An Integrated Shape Memory Alloy Micro-Actuator Controlled by Thermoelectric Effect, *Sens. Actuators A*, 2002, **99**, p 297–303
7. K.J. Gabriel, W.S.N. Trimmer, and J.A. Walzer, A Micro-Rotary Actuator Using Shape Memory Alloys, *Sens. Actuators A*, 1988, **15**, p 95–102
8. K. Kuribayashi, Millimeter-Sized Joint Actuator Using a Shape Memory Alloy, *Sens. Actuators A*, 1989, **20**, p 57–64
9. D. Grant and V. Hayward, *Design of a Shape Memory Alloy Actuator with High Strain and Variable Structure Control*, Proceedings 1995 IEEE International Conference on Robotics and Automation
10. K.T. Ulrich and S.D. Eppinger, *Product Design and Development*, McGraw-Hill, Columbus, OH, 2008
11. D.G. Ullman, *The Mechanical Design Process*, McGraw-Hill, Columbus, OH, 1997
12. I. Spinella and E. Dragoni, Design Equations for Binary Shape Memory Actuators Under Dissipative Forces, *J. Mech. Eng. Sci.*, 2009, **223**(C3), p 531–543
13. J.E. Shigley, C.R. Mischke, and T.H. Brown, *Standard Handbook of Machine Design*, McGraw-Hill, Columbus, OH, 2004
14. G. Niemann, *Machine Elements: Design and Calculation in Mechanical Engineering*, Springer, Berlin, 1978
15. H. Meier and C. Oelschlaeger, Numerical Thermomechanical Modeling of Shape Memory Alloy Wires, *Mater. Sci. Eng. A*, 2004, **378**, p 484–489